Generalizing the wavelet-based multifractal formalism to vector-valued random fields: application to turbulent velocity and vorticity 3D numerical data

Pierre Kestener[1,2] and Alain Arneodo[2]

[1]*CEA-Saclay, DSM/DAPNIA/SEDI, 91191 Gif-sur-Yvette, France*
[2]*Laboratoire de Physique, Ecole Normale Supérieure de Lyon, 46 allée d'Italie, 69364 Lyon cédex 07, France*
(Dated: March 12, 2004)

We use singular value decomposition techniques to generalize the wavelet transform modulus maxima method to the multifractal analysis of vector-valued random fields. The method is calibrated on synthetic multifractal 2D vector measures and monofractal 3D fractional Brownian vector fields. We report the results of some application to the velocity and vorticity fields issued from 3D isotropic turbulence simulations. This study reveals the existence of an intimate relationship between the singularity spectra of these two vector fields which are found significantly more intermittent than previously estimated from longitudinal and transverse velocity increment statistics.

The multifractal formalism was introduced in the context of fully-developed turbulence data analysis and modeling to account for the experimental observation of some deviation to Kolmogorov theory (K41) of homogenous and isotropic turbulence [1]. The predictions of various multiplicative cascade models, including the weighted curdling (binomial) model proposed by Mandelbrot [2], were tested using box-counting (BC) estimates of the so-called $f(\alpha)$ singularity spectrum of the dissipation field [3]. Alternatively, the intermittent nature of the velocity fluctuations were investigated via the computation of the $D(h)$ singularity spectrum using the structure function (SF) method [4]. Unfortunately, both types of studies suffered from severe insufficiencies. On the one hand, they were mostly limited by one point probe measurements to the analysis of one (longitudinal) velocity component and to some 1D surrogate approximation of the dissipation [5]. On the other hand, both the BC and SF methodologies have intrinsic limitations and fail to fully characterize the corresponding singularity spectrum since only the strongest singularities are a priori amenable to these techniques [6]. In the early nineties, a wavelet-based statistical approach was proposed as a unified multifractal description of singular measures and multi-affine functions [6]. Applications of the so-called *wavelet transform modulus maxima* (WTMM) method have already provided insight into a wide variety of problems, e.g., fully developed turbulence, econophysics, meteorology, physiology and DNA sequences [7, 8]. Later on, the WTMM method was generalized to 2D for multifractal analysis of rough surfaces [9], with very promising results in the context of the geophysical study of the intermittent nature of satellite images of the cloud structure [10, 11] and the medical assist in the diagnosis in digitized mammograms [11, 12]. Recently the WTMM method has been further extended to 3D analysis and applied to dissipation and enstrophy 3D numerical data issue from isotropic turbulence direct numerical simulations (DNS) [13, 14]. Thus far, the multifractal description has been mainly devoted to scalar measures and functions. In the spirit of a preliminary theoretical study of self-similar vector-valued measures by Falconer and O'Neil [15], our objective here is to generalize the WTMM method to vector-valued random fields with the specific goal to achieve a comparative 3D vectorial multifractal analysis of DNS velocity and vorticity fields.

Let us note $\mathbf{V}(\mathbf{x} = (x_1, x_2, .., x_d))$, a vector field with square integrable scalar components $V_j(\mathbf{x})$, $j = 1, 2, .., d$. Along the line of the 3D WTMM method [13, 14], let us define d wavelets $\psi_i(\mathbf{x}) = \partial\phi(\mathbf{x})/\partial x_i$ for $i = 1, 2, .., d$ respectively, where $\phi(\mathbf{x})$ is a scalar smoothing function well localized around $|\mathbf{x}| = 0$. The wavelet transform (WT) of $\mathbf{V}$ at point $\mathbf{b}$ and scale a is the following tensor [14]:

$$\mathbb{T}_{\boldsymbol{\psi}}[\mathbf{V}](\mathbf{b}, a) = \begin{pmatrix} T_{\psi_1}[V_1] & T_{\psi_1}[V_2] & ... & T_{\psi_1}[V_d] \\ T_{\psi_2}[V_1] & T_{\psi_2}[V_2] & ... & T_{\psi_2}[V_d] \\ \vdots & \vdots & & \vdots \\ T_{\psi_d}[V_1] & T_{\psi_d}[V_2] & ... & T_{\psi_d}[V_d] \end{pmatrix}, \quad (1)$$

where

$$T_{\psi_i}[V_j](\mathbf{b}, a) = a^{-d} \int d^d\mathbf{r} \, \psi_i\big(a^{-1}(\mathbf{r} - \mathbf{b})\big)V_j(\mathbf{r}). \quad (2)$$

In order to characterize the local Hölder regularity of $\mathbf{V}$, one needs to find the direction that locally corresponds to the maximum amplitude variation of $\mathbf{V}$. This can be obtained from the *singular value decomposition* (SVD) [16] of the matrix $(T_{\psi_i}[V_j])$ (Eq. (1)):

$$\mathbb{T}_{\boldsymbol{\psi}}[\mathbf{V}] = \mathbb{G}\Sigma\mathbb{H}^T, \quad (3)$$

where $\mathbb{G}$ and $\mathbb{H}$ are orthogonal matrices ($\mathbb{G}^T\mathbb{G} = \mathbb{H}^T\mathbb{H} = \mathbb{I}_d$) and $\Sigma = diag(\sigma_1, \sigma_2, .., \sigma_d)$ with $\sigma_i \geq 0$, for $1 \leq i \leq d$. The columns of $\mathbb{G}$ and $\mathbb{H}$ are referred to as the left and right singular vectors, and the singular values of $\mathbb{T}_{\boldsymbol{\psi}}[\mathbf{V}]$ are the non-negative square roots σ_i of the d eigenvalues of $\mathbb{T}_{\boldsymbol{\psi}}[\mathbf{V}]^T\mathbb{T}_{\boldsymbol{\psi}}[\mathbf{V}]$. Note that this decomposition is unique, up to some permutation of the σ_i's.

The direction of the largest amplitude variation of $\mathbf{V}$, at point $\mathbf{b}$ and scale a, is thus given by the eigenvector $\mathbf{G}_\rho(\mathbf{b}, a)$ associated to the spectral radius $\rho(\mathbf{b}, a) = \max_j \sigma_j(\mathbf{b}, a)$. One is thus led to the analysis of the vector field $\mathbf{T}_{\psi,\rho}[\mathbf{V}](\mathbf{b}, a) = \rho(\mathbf{b}, a)\mathbf{G}_\rho(\mathbf{b}, a)$. Following the WTMM analysis of scalar fields [9, 13, 14], let us define, at a given scale a, the WTMM as the position $\mathbf{b}$ where the modulus $\mathcal{M}_\psi[\mathbf{V}](\mathbf{b}, a) = |\mathbf{T}_{\psi,\rho}[\mathbf{V}](\mathbf{b}, a)| = \rho(\mathbf{b}, a)$ is locally maximum along the direction of $\mathbf{G}_\rho(\mathbf{b}, a)$. These WTMM lie on connected $(d-1)$ hypersurfaces called *maxima hypersurfaces* (see Figs 2b and 2c). In theory, at each scale a, one only needs to record the position of the local maxima of $\mathcal{M}_\psi$ (WTMMM) along the maxima hypersurfaces together with the value of $\mathcal{M}_\psi[\mathbf{V}]$ and the direction of $\mathbf{G}_\rho$. These WTMMM are disposed along connected curves across scales called *maxima lines* living in a $(d+1)$ space $(\mathbf{x}, a)$. The WT skeleton is then defined as the set of maxima lines that converge to the $(x_1, x_2, .., x_d)$ hyperplane in the limit $a \to 0^+$ (see Fig. 2d). The local Hölder regularity of $\mathbf{V}$ is estimated from the power-law behavior $\mathcal{M}_\psi[\mathbf{V}]\big(\mathcal{L}_{\mathbf{r}_0}(a)\big) \sim a^{h(\mathbf{r}_0)}$ along the maxima line $\mathcal{L}_{\mathbf{r}_0}(a)$ pointing to the point $\mathbf{r}_0$ in the limit $a \to 0^+$, provided the Hölder exponent $h(\mathbf{r}_0)$ be smaller than the number n_ψ of zero moments of the analyzing wavelet ψ [17]. As for scalar fields [6, 9, 13], the tensorial WTMM method consists in defining the partition functions:

$$\mathcal{Z}(q, a) = \sum_{\mathcal{L} \in \mathcal{L}(a)} \left(\mathcal{M}_\psi[\mathbf{V}](\mathbf{r}, a)\right)^q \sim a^{\tau(q)}, \qquad (4)$$

where $q \in \mathbb{R}$ and $\mathcal{L}(a)$ is the set of maxima lines that exist at scale a in the WT skeleton. Then by Legendre transforming $\tau(q)$, one gets the singularity spectrum $D(h) = \min_q(qh - \tau(q))$, defined as the Hausdorff dimension of the set of points $\mathbf{r}$ where $h(\mathbf{r}) = h$. Alternatively, one can compute the mean quantities:

$$h(q, a) = \sum_{\mathcal{L} \in \mathcal{L}(a)} \ln|\mathcal{M}_\psi[\mathbf{V}](\mathbf{r}, a)| \; W_\psi[\mathbf{V}](q, \mathcal{L}, a) ,$$
$$\tag{5}$$
$$D(q, a) = \sum_{\mathcal{L} \in \mathcal{L}(a)} W_\psi[\mathbf{V}](q, \mathcal{L}, a) \; \ln\big(W_\psi[\mathbf{V}](q, \mathcal{L}, a)\big) ,$$

where $W_\psi[\mathbf{V}](q, \mathcal{L}, a) = \big(\mathcal{M}_\psi[\mathbf{V}](\mathbf{r}, a)\big)^q / \mathcal{Z}(q, a)$ is a Boltzmann weight computed from the WT skeleton. From the scaling behavior of these quantities, one can extract $h(q) = \lim_{a \to 0^+} h(q, a)/\ln a$ and $D(q) = \lim_{a \to 0^+} D(q, a)/\ln a$ and therefore the $D(h)$ spectrum.

As a test application of this extension of the WTMM method to the vector situation, let us consider the self-similar 2D vector measures supported by the unit square defined in Ref. [15]. As sketched in Fig. 1, from step n to step $n+1$, each square is divided into 4 identical sub-squares and for each of these sub-squares, one defines a similitude S_i that transforms the vector $\mathbf{V}^{(n)}$ at step n into the vector $\mathbf{V}_i^{(n+1)}$ for the sub-square i at step $n+1$. The σ-additivity property of positive scalar measures is
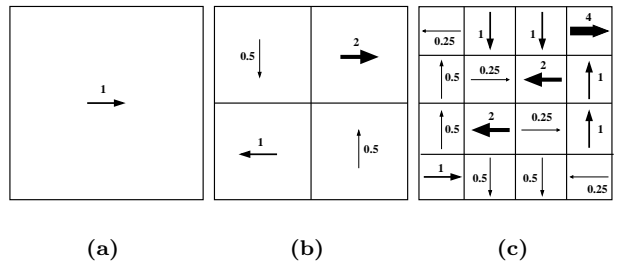

FIG. 1: First construction steps of a singular vector-valued measure supported by the unit square. The norm of the four similitude S_i are $p_1 = p_4 = 1/2$, $p_2 = 2$ and $p_3 = 1$ [15].

now replaced by the vectorial additivity condition $\mathbf{V}^{(n)} = \sum_{i=1}^4 \mathbf{V}_i^{(n+1)}$. A straightforward calculation yields the following analytical expression for the partition function scaling exponents $\tau(q)$ (Eq. (4)):

$$\tau(q) = -\log_2(p_1^q + p_2^q + p_3^q + p_4^q) - q, \qquad (6)$$

where p_i ($i = 1$ to 4), are the norms of the similitudes S_i. Note that this formula is identical to the theoretical spectrum of a non-conservative scalar multinomial measure distributed on the unit square with the weights p_i [13, 14]. Indeed, if the construction process in Fig. 1 is conservative from a vectorial point of view, it does not conserve the norm of the measure: $\sum_{i=1}^4 p_i = 4 > 1$. From Legendre transforming Eq. (6), one gets a $D(h)$ singularity spectrum with a characteristic multifractal single-humped shape (see Fig. 3d) supported by the interval $[h_{\min}, h_{\max}] = [-1 - \log_2(\max_i p_i), -1 - \log_2(\min_i p_i)]$ and whose maximum $D_F = -\tau(0) = 2$ is the signature that the considered vector-valued measure is almost everywhere singular on the unit square.

In Fig. 2 are illustrated the main steps of our tensorial WT methodology when applied to 16 $(1024)^2$ realizations of a random generalization of the vectorial multiplicative construction process described in Fig. 1. Focusing on the central $(128)^2$ sub-square, we show the singular vector-valued measure (Fig. 2a) and the corresponding WTMM chains computed with a first order analyzing wavelet at two different scales (Figs 2b and 2c). On these maxima chains, the black dots correspond to the location of the WTMMM at these scales. The size of the arrows that originate from each black dot is proportional to the spectral radius $\rho(\mathbf{b}, a)$ and its direction is along the eigenvector $\mathbf{G}_\rho(\mathbf{b}, a)$. When linking these WTMMM across scales, one gets the set of maxima lines shown in Fig. 2d as defining the WT skeleton. In Fig. 3 are reported the results of the computation of the multifractal spectra (annealed averaging). As shown in Fig. 3a, $\mathcal{Z}(q, a)$ (Eq. (4)) display nice scaling behavior over four octaves (when plotted versus a in a logarithmic representation), for $q \in]-2, 4[$ for which statistical convergence turns out to be achieved. A linear regression fit of the
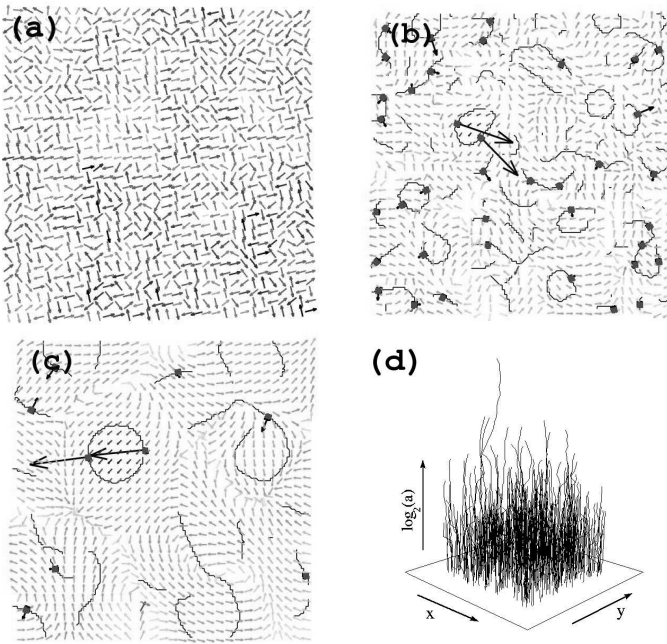
FIG. 2: 2D WT analysis of the 2D vector-valued self-similar measure shown in Fig. 1 but with systematic random permutation of the S_i. ψ is a first-order analyzing wavelet ($\phi(\mathbf{r})$ is the Gaussian). (a) 32 grey-scale coding of the central $(128)^2$ portion of the original $(1024)^2$ field. In (b) $a = 2^2\sigma_W$ and (c) $a = 2^3\sigma_W$, are shown the maxima chains; from the local maxima (WTMMM) of $\mathcal{M}_\psi$ along these chains (■) originates a black arrow whose length is proportional to $\mathcal{M}_\psi$ and direction is along $\mathbf{T}_{\psi,\rho}[\mathbf{V}]$. (d) WT skeleton obtained by linking the WTMMM across scales. $\sigma_W = 7$ (pixels) is the characteristic size of ψ at the smallest resolved scale.

FIG. 3: Multifractal analysis of the 2D vector-valued random measure field using the 2D tensorial WTMM method (□) and BC techniques (■). (a) $\log_2 \mathcal{Z}(q,a)$ vs $\log_2 a$; (b) $h(q,a)$ vs $\log_2 a$; the solid lines correspond to linear regression fits over $\sigma_W \lesssim a \lesssim 2^4\sigma_W$. (c) $\tau(q)$ vs q; the solid line corresponds to the theoretical prediction (Eq. (6)). (d) $D(h)$ vs h; the solid line is the Legendre transform of Eq. (6).

data yields the nonlinear $\tau(q)$ spectrum shown in Fig. 3c, in remarkable agreement with the theoretical spectrum (Eq. (6)). This multifractal diagnosis is confirmed in Fig. 3b where the slope of $h(q,a)$ (Eq. (5)) versus $\log_2 a$, clearly depends on q. From the estimate of $h(q)$ and $D(q)$ (Eq. (5)), one gets the single-humped $D(h)$ curve shown in Fig. 3d which matches perfectly the theoretical $D(h)$ spectrum. In Fig. 3, we have reported for comparison, the results obtained when using a box-counting (BC) algorithm adapted to the multifractal analysis of singular vector-valued measures [14, 15, 18]. There is no doubt that BC provides much poorer results, especially concerning the estimates of $\tau(q)$, $h(q)$ and $D(q)$ for negative q values. This deficiency mainly results from the fact that the vectorial resultant may be very small whereas the norms of the vector measures in the sub-boxes are not small at all. The results reported in Fig. 3 bring the demonstration that our tensorial WTMM methodology paves the way from multifractal analysis of singular scalar measures to singular vector measures.

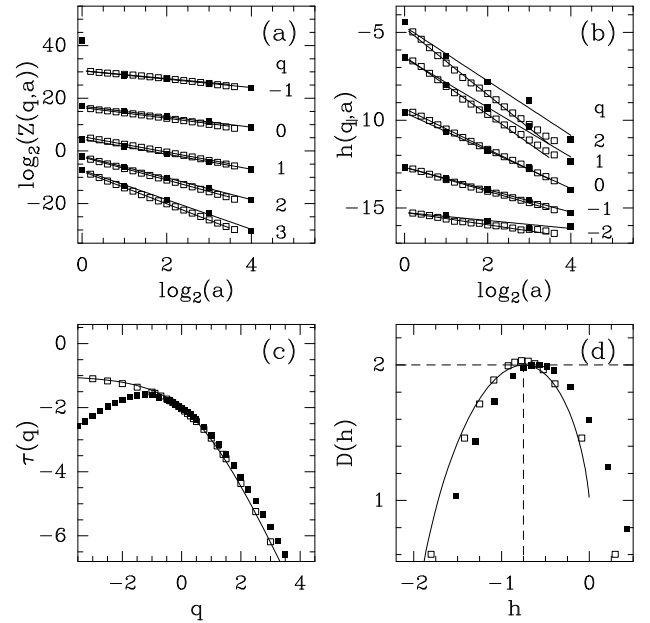In Fig. 4 are reported the results of the application of our tensorial WTMM method to isotropic turbulence DNS data obtained by Lévêque. This comparative 3D multifractal analysis of the velocity ($\mathbf{v}$) and vorticity ($\boldsymbol{\omega}$) fields corresponds to some averaging over 18 snapshots of $(256)^3$ DNS run at $R_\lambda = 140$. As shown in Figs. 4a and 4b, both the $\mathcal{Z}(q,a)$ and $h(q,a)$ partition functions display rather nice scaling properties for $q = -4$ to 6, except at small scales ($a \lesssim 2^{1.5}\sigma_W$) where some curvature is observed in the log-log plots likely induced by dissipation effects [1, 19]. Linear regression fit of the data (Fig. 4a) in the range $2^{1.5}\sigma_W \leq a \leq 2^{3.9}\sigma_W$ yields the nonlinear $\tau_{\mathbf{v}}(q)$ and $\tau_{\boldsymbol{\omega}}(q)$ spectra shown in Fig. 4c, the hallmark of multifractality. For the vorticity field, $\tau_{\boldsymbol{\omega}}(q)$ is a decreasing function similar to the one obtained for the singular vector-valued measure in Fig. 3c; hence $h(q)(= \partial\tau(q)/\partial q) < 0$ and the support of the $D(h)$ singularity spectrum expands over negative h values as shown in Fig. 4d. In contrast $\tau_{\mathbf{v}}(q)$ is an increasing function which implies that $h(q) > 0$ as the signature that $\mathbf{v}$ is a continuous function. Let us point out that the so-obtained $\tau_{\mathbf{v}}(q)$ curve significantly departs from the linear behavior obtained for 18 $(256)^3$ realizations of vector-valued fractional Brownian motions $\mathbf{B}^{1/3}$ of index $H = 1/3$, in good agreement with the theoretical spectrum $\tau_{\mathbf{B}^{1/3}}(q) = q/3 - 3$. But even more remarkable, the results reported in Fig. 4b for $h(q,a)$ suggest, up to statistical uncertainty, the validity of the relationship $h_{\boldsymbol{\omega}}(q) = h_{\mathbf{v}}(q) - 1$. Actually, as shown in Fig. 4d, $D_{\boldsymbol{\omega}}(h)$ and $D_{\mathbf{v}}(h)$ curves are likely to coincide after translating the later by one unit on the left. This
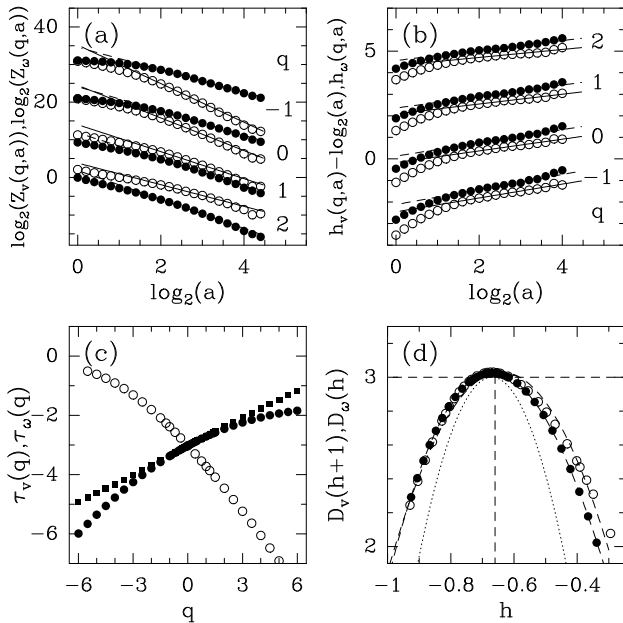
FIG. 4: Multifractal analysis of Lévêque DNS velocity ($\bullet$) and vorticity ($\circ$) fields ($d = 3$, 18 snapshots) using the tensorial 3D WTMM method; the symbols ($\blacksquare$) correspond to a similar analysis of vector-valued fractional Brownian motions, $\mathbf{B}^{H=1/3}$. (a) $\log_2 \mathcal{Z}(q,a)$ vs $\log_2 a$; (b) $h_\omega(q,a)$ vs $\log_2 a$ and $h_\mathbf{v}(q,a) - \log_2 a$ vs $\log_2 a$; the solid and dashed lines correspond to linear regression fits over $2^{1.5}\sigma_W \lesssim a \lesssim 2^{3.9}\sigma_W$. (c) $\tau_\mathbf{v}(q)$, $\tau_\omega(q)$ and $\tau_{\mathbf{B}^{1/3}}(q)$ vs q; (d) $D_\mathbf{v}(h+1)$, $D_\omega(h)$ vs h; the dashed lines correspond to log-normal regression fits with the parameter values $C_2^\mathbf{v} = 0.049$ and $C_2^\omega = 0.055$; the dotted line is the experimental singularity spectrum ($C_2^{\delta v_\parallel} = 0.025$) for 1D longitudinal velocity increments [19].

is to our knowledge the first numerical evidence that the singularity spectra of $\mathbf{v}$ and ω might be so intimately related: $D_\mathbf{v}(h+1) = D_\omega(h)$ (a result that could have been guessed intuitively by noticing that $\omega = \nabla \wedge \mathbf{v}$ involves first order derivatives only). Finally, let us note that, for both fields, the $\tau(q)$ and $D(h)$ data are quite well fitted by log-normal parabolic spectra [19]:

$$
\begin{aligned}
\tau(q) &= -C_0 - C_1 q - C_2 q^2/2\,, \\
D(h) &= C_0 - (h + C_1)^2/2C_2\,.
\end{aligned}
\tag{7}
$$

Both fields are found singular almost everywhere: $C_0^\mathbf{v} = -\tau_\mathbf{v}(q=0) = D_\mathbf{v}(q=0) = 3.02 \pm 0.02$ and $C_0^\omega = 3.01 \pm 0.02$. The most frequent Hölder exponent $h(q = 0) = -C_1$ (corresponding to the maximum of $D(h)$) takes the value $-C_1^\mathbf{v} \simeq -C_1^\omega + 1 = 0.34 \pm 0.02$. Indeed, this estimate is much closer to the K41 prediction $h = 1/3$ [1] than previous experimental measurements ($h = 0.39 \pm 0.02$) based on the analysis of longitudinal velocity fluctuations [19]. Consistent estimates are obtained for C_2 (that characterizes the width of $D(h)$): $C_2^\mathbf{v} = 0.049 \pm 0.003$ and $C_2^\omega = 0.055 \pm 0.004$. Note that these values are much larger than the experimental estimate $C_2 = 0.025 \pm 0.003$ derived for 1D longitudinal

velocity increment statistics [19]. Actually they are comparable to the value $C_2 = 0.040$ extracted from experimental transverse velocity increments [19b].

To conclude, we have generalized the WTMM method to vector-valued random fields. Preliminary applications to DNS turbulence data have revealed the existence of an intimate relationship between the velocity and vorticity 3D statistics that turn out to be significantly more intermittent than previously estimated from 1D longitudinal velocity increments statistics. This new methodology looks very promising to many extents. Thanks to the SVD, one can focus on fluctuations that are locally confined in 2D ($\min_i \sigma_i = 0$) or in 1D (the two smallest σ_i are zero) and then simultaneously proceed to a multifractal and structural analysis of turbulent flows. The investigation along this line of vorticity sheets and vorticity filaments in DNS is in current progress. We are very grateful to E. Lévêque for allowing us to have access to his DNS data and to the CNRS under GDR turbulence.

[1] U. Frisch, *Turbulence* (Cambridge Univ. Press, Cambridge, 1995).
[2] B. B. Mandelbrot, J. Fluid Mech. **62**, 331 (1974).
[3] C. Meneveau and K. R. Sreenivasan, J. Fluid Mech. **224**, 429 (1991).
[4] G. Parisi and U. Frisch, in *Turbulence and Predictability in Geophysical Fluid Dynamics and Climate Dynamics*, edited by M. Ghil *et al.* (North-Holland, Amsterdam, 1985), p. 84.
[5] E. Aurell *et al.*, J. Fluid Mech. **238**, 467 (1992).
[6] J. F. Muzy, E. Bacry, and A. Arneodo, Phys. Rev. E **47**, 875 (1993); Int. J. of Bifurcation and Chaos **4**, 245 (1994); A. Arneodo, E. Bacry, and J. F. Muzy, Physica A **213**, 232 (1995).
[7] A. Arneodo *et al.*, *Ondelettes, Multifractales et Turbulences : de l'ADN aux croissances cristallines* (Diderot Editeur, Art et Sciences, Paris, 1995).
[8] *The Science of Disasters : climate disruptions, heart attacks and market crashes*, edited by A. Bunde, J. Kropp, and H. Schellnhuber (Springer Verlag, Berlin, 2002).
[9] A. Arneodo, N. Decoster and S. G. Roux, Eur. Phys. J. B **15**, 567 (2000); N. Decoster, S. G. Roux, and A. Arneodo, Eur. Phys. J. B **15**, 739 (2000).
[10] A. Arneodo, N. Decoster, and S. G. Roux, Phys. Rev. Lett. **83**, 1255 (1999). S. G. Roux, A. Arneodo, and N. Decoster, Eur. Phys. J. B **15**, 765 (2000).
[11] A. Arneodo *et al.*, Advances in Imaging and Electron Physics, **126**, 1 (2003).
[12] P. Kestener *et al.*, Image Anal. Stereol. **20**, 169 (2001).
[13] P. Kestener and A. Arneodo, Phys. Rev. Lett. **91**, 194501 (2003).
[14] P. Kestener, Ph.D. thesis, University of Bordeaux I, 2003.
[15] K. J. Falconer and T. C. O'Neil, Proc. R. Soc. Lond. A **452**, 1433 (1996).
[16] G. H. Golub and C. V. Loan, *Matrix Computations*, 2nd ed. (John Hopkins University Press, Baltimore, 1989).
[17] Note that if $h_i(\mathbf{r}_0)$ are the Hölder exponents of the d scalar components $V_i(\mathbf{r}_0)$ of $\mathbf{V}$, then $h(\mathbf{r}_0) = \min_i h_i(\mathbf{r}_0)$.

[18] We recall the relationship $h = \alpha - d$, between the Hölder exponent h and the singularity exponent α generally obtained by BC techniques ($D(\alpha - d) = f(\alpha)$).

[19] (a) A. Arneodo, S. Manneville, and J. F. Muzy, Eur. Phys. J. B **1**, 129 (1998); (b) Y. Malécot *et al.*, Eur. Phys. J. B **16**, 549 (2000); (c) J. Delour, J. F. Muzy, and A. Arneodo, Eur. Phys. J. B **23**, 243 (2001).